Applied and Environmental Microbiology, Sept. 2008, p. 5457–5465 Vol. 74, No. 17
0099-2240/08/$08.00+0 doi:10.1128/AEM.02075-07

Use of Atomic Force Microscopy and Transmission Electron Microscopy for Correlative Studies of Bacterial Capsules▽†

Oleg Stukalov,[1,3] Anton Korenevsky,[2,3] Terry J. Beveridge,[2,3] and John R. Dutcher[1,3]*

Department of Physics,[1] Department of Molecular and Cellular Biology,[2] and Advanced Foods and Materials Network, Networks of Centres of Excellence,[3] University of Guelph, Guelph, Ontario, Canada N1G 2W1

Received 11 September 2007/Accepted 18 June 2008

Bacteria can possess an outermost assembly of polysaccharide molecules, a capsule, which is attached to their cell wall. We have used two complementary, high-resolution microscopy techniques, atomic force microscopy (AFM) and transmission electron microscopy (TEM), to study bacterial capsules of four different gram-negative bacterial strains: *Escherichia coli* K30, *Pseudomonas aeruginosa* FRD1, *Shewanella oneidensis* MR-4, and *Geobacter sulfurreducens* PCA. TEM analysis of bacterial cells using different preparative techniques (whole-cell mounts, conventional embeddings, and freeze-substitution) revealed capsules for some but not all of the strains. In contrast, the use of AFM allowed the unambiguous identification of the presence of capsules on all strains used in the present study, including those that were shown by TEM to be not encapsulated. In addition, the use of AFM phase imaging allowed the visualization of the bacterial cell within the capsule, with a depth sensitivity that decreased with increasing tapping frequency.

Polysaccharides are produced by bacteria of diverse genera. Those of gram-negative bacteria can be classified either as capsular polysaccharide (CPS) molecules, which are typically covalently attached to the outer membrane of the cell wall through a hydrophobic moiety, or extracellular polysaccharide, which is exported by the bacterium to form the main component in extracellular polymeric substances (EPS) (30). CPS is produced by the cell in response to environmental conditions. When CPS is present, it often forms the outermost peripheral structure of the cells and therefore mediates interactions between the cell and its environment. A capsule is useful to the cell for several reasons: it can increase the cell's virulence, adhere the cell to various surfaces (19, 33), prevent desiccation under low humidity (28), and provide a polymeric network for the storage of nutrients (30) or the retention of toxic agents (17).

A broad range of techniques is currently available for the detection and visualization of bacterial capsules. These include nonmicroscopy techniques, such as serological reactions, molecular biological approaches, and virological identification (3). Light microscopy with nonspecific stain or label, e.g., nigrosin, India ink, or cationized ferritin, or specific stain or label, e.g., antibodies and fluorescent lectins, is an important laboratory tool for the identification of the presence of capsules (5). Most of these techniques can be used on unfixed, fully hydrated cells in solution. However, since the spatial resolution limit of a light microscope when using these staining techniques is rarely less than 500 nm, it is difficult to detect the presence of bacterial capsules with thicknesses that are below this optical resolution limit. Although fluorescent tagging of the capsules can allow the detection of the presence of very thin bacterial capsules, this requires specific staining or labeling, which is not always possible.

For decades, transmission electron microscopy (TEM) has been a strong research tool in microbiology for high-resolution structural studies of bacteria and their components (6). Since CPS is highly hydrated with water, often with hydration in excess of 95% by mass, stabilization and staining are necessary during sample preparation for TEM in an attempt to preserve the original structure and enhance the contrast of CPS (4). The simplest TEM technique involves the preparation of whole-cell mounts, in which bacterial cells are dried onto thin, free-standing films of Formvar, and this is normally followed by staining with heavy metals (6). The whole-cell mount TEM technique is widely used to study the morphology of bacterial cells and their surface structures, such as flagella and pili. TEM of thin sections of cells stained with Ruthenium red (RR), Alcian blue (21), or cationized ferritin (3) reveals the presence of capsules on bacteria. Such staining, however, requires that the CPS polymers have a negative charge, and therefore it is not reliable for CPS with a neutral, positive, or small charge. Freeze substitution is the most reliable TEM technique (18, 22) for observing bacterial capsules, due to the rapid physical vitrification of cells which fixes them in a fully hydrated state and results in very good preservation of the native structure of the cell (6). However, the use of the freeze-substitution technique has so far been limited, since it is laborious and time-consuming and requires specialized equipment.

Atomic force microscopy (AFM) has recently been used in microbiological studies (see reference 14 for a recent review) to obtain three-dimensional topographical images of individual bacterial cells, both in air and under physiological conditions (8, 27, 36), and to visualize cell wall structures like S-layer proteins (31) and peptidoglycan sacculi (45). Single-molecule resolution can be achieved using AFM with the proper choice of experimental conditions, e.g., sample preparation, sample environment, and cantilever tip shape (14). Another advantage

* Corresponding author. Mailing address: Department of Physics, University of Guelph, 50 Stone Rd. E, Guelph, Ontario, Canada N1G 2W1. Phone: (519) 824-4120. Fax: (519) 836-9967. E-mail: dutcher@physics.uoguelph.ca.

† This work is dedicated to T.J.B., our good friend and superb colleague, who passed away during the preparation of the manuscript.

▽ Published ahead of print on 7 July 2008.

of the AFM technique is the ability to directly probe the mechanical and adhesive properties of bacterial cells by measuring force-distance (FD) curves (9). FD curves allow the determination of interaction forces between the AFM tip and a bacterial cell and its cell wall components with a force resolution as small as tens of piconewtons (37, 39) and in principle allow the determination of the turgor pressure within the bacterium (2, 44). All of these capabilities make AFM a unique tool in microbiology, and it is especially powerful when it is used in combination with complementary microscopic and biophysical techniques (38).

The properties of microbial polysaccharides (PS) have been studied using AFM (see reference 34 for a recent review), and the visualization and characterization of the conformation of a single isolated PS molecule have been demonstrated (12). It was suggested that the presence of CPS can be inferred from the interactions between the AFM tip and bacteria immobilized on an underlying substrate (15), or between bacteria attached to the AFM tip and the underlying substrate (39). Schaer-Zammaretti and Ubbink (32) assumed that the large adhesion forces measured between an AFM cantilever and lactic acid bacterium in liquid medium corresponded to the interaction of the AFM tip with CPS, implying that AFM can be used to detect the presence of bacterial capsules. However, the inference of the presence of bacterial capsules through the measurement of adhesive forces has significant disadvantages. The adhesion forces measured between AFM tips and bacteria depend on many different factors, such as the chemical composition and length of the CPS polymers and the surface properties of the AFM cantilever. In addition, it has been shown (19) that CPS can also inhibit adhesion, instead of promoting it, clearly indicating that measurements of AFM tip adhesion to CPS molecules are sample dependent.

In the present study, we report the systematic, direct observation of capsules on a diverse range of gram-negative bacteria using AFM and TEM techniques. *Escherichia coli* K30 is a model strain for which the molecular mechanisms of CPS synthesis have been studied in detail (43). *Pseudomonas aeruginosa* FRD1 is a mucoid clinical isolate important in the pathogenesis of cystic fibrosis which under certain conditions produces copious amounts of alginate CPS (25). *Shewanella* and *Geobacter* spp. are important bacteria in natural environments because of their ability to reduce metals (24). *Shewanella* spp. can also be opportunistic pathogens (26), and they can be responsible for food spoilage (42). The presence of capsules surrounding certain strains of *Shewanella* has been reported (22), and the importance of capsules for metal reduction by mediating bacterial adhesion was suggested (23). We have chosen to study *S. oneidensis* MR-4 bacteria because the molecular structures of the lipopolysaccharide and CPS have been recently characterized (41). The presence of capsular material for *Geobacter sulfurreducens* cells has not been observed previously; only the molecular structure of the core region of its lipopolysaccharide has been reported (40).

MATERIALS AND METHODS

Bacterial strains and growth conditions. *Escherichia coli* K30 and *Pseudomonas aeruginosa* FRD1 were provided by C. Whitfield and J. Lam (Dept. of Cellular and Molecular Biology, University of Guelph, Guelph, ON, Canada), *Shewanella oneidensis* MR-4 was provided by D. Lies (Jet Propulsion Laboratory, Pasadena, CA), and *Geobacter sulfurreducens* PCA was from D. Lovley (Dept. of Microbiology, University of Massachusetts, Amherst). All cultures were grown aerobically (except *G. sulfurreducens* PCA, which was grown under strict anaerobic conditions) on a rotary shaker (150 rpm) and were harvested at mid-exponential growth phase (optical density at 470 nm, ~0.8). *E. coli* K30 and *P. aeruginosa* FRD1 were grown in Luria-Bertani medium at 37°C. *S. oneidensis* MR-4 was cultured at 24°C on tryptic soy broth. *G. sulfurreducens* PCA was grown at 30°C in modified NBAF medium prepared according to the procedure described in reference 11.

TEM. Whole-cell mounts were prepared using cells suspended in growth medium which was not centrifuged, since centrifugation may disrupt fine bacterial structures like pili, flagella, and capsules (29). A droplet of the bacterial suspension was placed onto a 50-nm-thick Formvar film that had been transferred onto a copper index TEM grid (Marivac, Canada). After waiting for ~15 min, the remaining solution was wicked away using a piece of filter paper. The samples were then rinsed with 2 ml of 2 mM HEPES buffer (pH 6.8) followed by a rinse with 1 ml of MilliQ water. The samples were then stained by placing a drop of 0.5% (wt/vol) uranyl acetate onto the samples and removing the excess by wicking with filter paper after 3 to 5 min. For the embedding of cells for thin sections, the glutaraldehyde-osmium tetroxide protocol detailed in reference 6 was followed and cells were embedded in LR white. Ruthenium red was also used to contrast CPS, as suggested by Beveridge et al. (6) For freeze-substitution preparations, each bacterial suspension was injected into thin copper specimen tubes (inner diameter, 350 μm; Leica), and the tubes were then flash-frozen in a high-pressure freezer (Leica EM Pact) according to the procedure described for planktonic cells by Hunter et al. (20). Freeze substitution was carried out in a Leica EMAFS unit (Leica Microsystems, Bannockburn, IL). Specimens were imaged using a Philips CM10 TEM operating at 100 kV under standard operating conditions. Whole-cell mounts, conventional embeddings, and freeze-substitution preparations were used for TEM experiments on all of the strains.

AFM. Bacteria were imaged using AFM under both hydrated (liquid) and anhydrous (air) conditions. For measurements in liquid, bacteria were immobilized on glass slides coated with poly-L-lysine (27) and rinsed with 1 ml of HEPES buffer. The glass slides were then immediately covered with HEPES buffer and transferred to the AFM. For AFM measurements of bacteria in air, the TEM whole mounts procedure described above was followed using freshly cleaved mica as the substrate. Two sets of AFM control experiments were performed. In one, we tested the difference between imaging bacteria prepared from suspension in HEPES buffer versus MilliQ water. For this, bacteria were washed in HEPES or MilliQ water as the liquid agent. Bacteria were allowed to dry for 15 to 20 min, and AFM measurements were then performed in air. A second set of control experiments was performed to measure the effect of drying the bacteria and their capsules in air. Bacteria were dried onto mica and measured by AFM; the samples were then left for periods of up to 14 h in the AFM without a change in the position of the cantilever and then remeasured. All sample preparations were performed under ambient conditions except those for the *Geobacter* bacteria, for which the samples were prepared in a glove box under anaerobic conditions and then immediately transferred to the AFM for measurement in air.

A Dimension 3100 (Veeco/Digital Instruments, CA) AFM with silicon cantilevers (AC160TS; resonance frequency $f_0 \approx 300$ kHz, spring constant $k \approx 42$ N/m; Olympus, Japan) was used for high-frequency tapping mode AFM measurements in air. AFM contact mode images in liquid (HEPES buffer), as well as low-frequency tapping mode images in air, were collected using a MFP-3D AFM (Asylum Research, CA). The AFM measurements in HEPES buffer were performed using CSC38 contact silicon cantilevers (cantilever B; MikroMasch, Estonia; $f_0 \approx 10$ kHz, $k \approx 0.03$ N/m). SCS37 cantilevers (cantilever B; MikroMasch, Estonia; $f_0 \approx 21$ kHz, $k \approx 0.3$ N/m) were used to obtain the low-frequency tapping mode images. The thermal spectra method incorporated in the MFP-3D software was used for the calibration of the force constant of the cantilevers. All of the AFM images were analyzed using the FemtoScan Online software (Advanced Technologies Center, Moscow, Russia).

Typically, two different tapping mode AFM images (topography and phase) were collected simultaneously (10). In phase imaging, the absolute phase of the cantilever vibrations is measured, with the phase of the driving signal at the resonance frequency of the cantilever assigned as zero in the Nanoscope software of the Dimension 3100 AFM. Phase images are typically constructed in the following manner: the darkest pixel and lightest pixel of the phase image are assigned to zero phase and maximum phase, respectively, allowing the construction of a gray-scale phase image. The value of the maximum phase varied from 20° to 50°, depending on the particular sample and cantilever and, to a lesser extent, on scanning conditions, such as scan rate and amplitude set point. Due to the relatively large height of the bacteria (typically 0.25 to 0.4 μm), the vertical scale of the images was so large that it was difficult to observe fine details in the

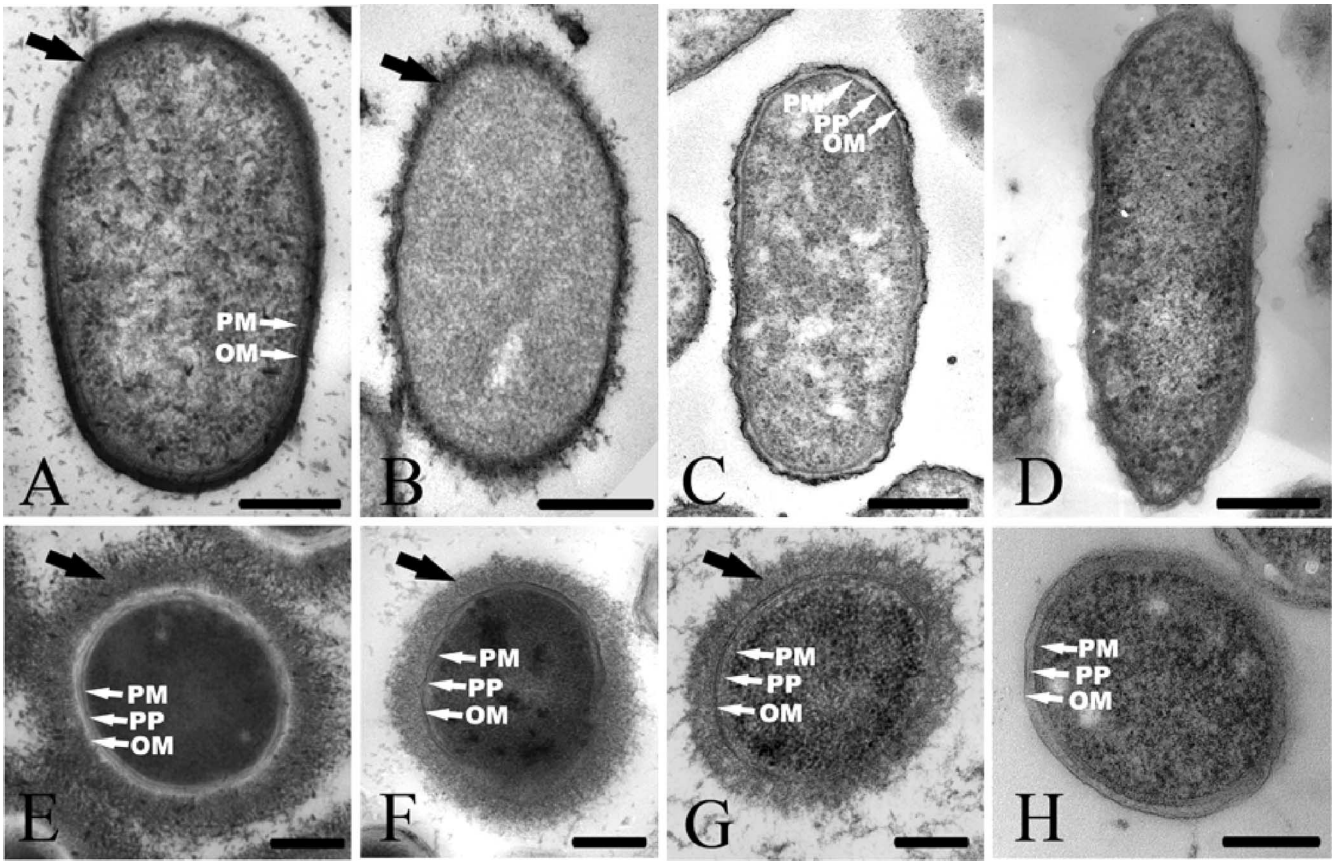

FIG. 1. Representative TEM images of thin sections of *E. coli* K30 (A and E), *P. aeruginosa* FRD1 (B and F), *S. oneidensis* MR-4 (C and G), and *G. sulfurreducens* PCA (D and H). The samples were prepared by conventional embeddings with Ruthenium red staining (A to D) and freeze-substitution (E to H). The black arrows indicate the bacterial capsule, and the white arrows indicate the plasma membrane (PM), periplasm (PP), and outer membrane (OM). Bars, 250 nm.

images. A derivative filter available in the FemtoScan Online software was sometimes applied to the images to enhance contrast.

AFM and TEM measurements on the same cells. TEM images of unstained whole mounts on TEM grids were collected, and the *x* and *y* coordinates were recorded so that the same cells could be measured using AFM. The optical microscope in the AFM was used to determine the *x* and *y* coordinates and therefore to identify the cells that had been previously imaged using TEM. Corresponding AFM images of these cells were collected. The TEM grids were then removed from the AFM and stained using uranyl acetate, and the same bacterial cells were imaged again using the AFM. Finally, the TEM grids were transferred back to the TEM and images of the same cells were collected.

RESULTS

TEM measurements of conventionally embedded and freeze-substituted samples. TEM images for conventionally embedded preparations of all strains used in the present study revealed fine details of the cell envelope, including the plasma membrane, the outer membrane, and the periplasm (Fig. 1A, B, C, and D). However, no capsules were observed for any of the strains unless the RR stain was used. Even with the use of the RR stain, capsules were not observed for all bacterial strains. Capsules were observed for *E. coli* K30 and *P. aeruginosa* FRD1 (Fig. 1A and B), but they were not observed for *S. oneidensis* MR-4 and *G. sulfurreducens* PCA (Fig. 1C and D). Capsules of *E. coli* K30 and *P. aeruginosa* FRD1 were similar in thickness (20 to 30 nm) but differed in appearance: those of K30 were compacted and appeared as a relatively dense mantle around the cells (Fig. 1A), whereas those of FRD1 appeared as a more fibrous layer (Fig. 1B). Difficulties associated with visualizing capsules using conventional embeddings have been reported previously (3, 21) and were attributed to the collapse of the delicate CPS molecules during sample preparation.

Compared with the conventionally embedded samples, the freeze-substitution sample preparation procedure resulted in better preservation of cell structures, with a distinct plasma membrane and outer membrane separated by periplasm (Fig. 1E, F, G, and H). Capsules were observed for all strains except for *G. sulfurreducens* PCA. There was a significant variation in the amount of capsule expression observed for the cells of each strain, ranging from cells with no capsule (nonencapsulated bacteria) to those with capsules extending up to 500 nm away from the cell. Such heterogeneity in the length of the CPS molecules is in agreement with previous observations (4, 18). For most of the freeze-substitution preparations in the present study, the capsules in the TEM images covered the cells uniformly, in agreement with observations by Bayer and Thurow (3), who used conventional embedding preparations of *E. coli* and stabilized the capsules by using high concentrations of anticapsule immunoglobulin G antibodies. The cells in the

freeze-substitution preparations in the present study had capsules with lower electron densities and greater thicknesses (150 to 250 nm) than those measured for the conventionally embedded samples using the RR stain. Capsular material in freeze-substituted cells was randomly arranged in a net-like mesh (Fig. 1E, F, and G).

TEM of cells stained with uranyl acetate. TEM measurements of bacteria stained with uranyl acetate (a negative stain commonly used in TEM sample preparations [6]) are commonly used to quickly assess cell dimensions and their surface structures, such as pili and flagella. In the present study, TEM measurements of stained bacteria revealed rod-shaped cells with the following average lengths and widths (means ± standard errors of the means): 2.3 ± 0.4 μm and 0.5 ± 0.1 μm for both *Shewanella* and *Pseudomonas*, 1.7 ± 0.4 μm and 0.9 ± 0.2 μm for *E. coli* K30, and 2.5 ± 0.5 and 0.49 ± 0.08 μm for *G. sulfurreducens*. Intact flagella and pili were typically observed for all preparations, and most of the cells appeared to be nonencapsulated.

TEM and AFM measurements of the same cells before and after staining with uranyl acetate. Since TEM measurements of stained bacteria did not reveal the presence of capsules, we decided to test whether this result could be attributed to the use of the uranyl acetate stain. For this test, we performed both TEM and AFM measurements on whole-mount preparations of *S. oneidensis* MR-4 bacteria before and after staining with uranyl acetate. Representative TEM and AFM results are shown in Fig. 2 for the same *S. oneidensis* MR-4 cell.

TEM measurements of whole mounts of cells (without the uranyl acetate stain) did not reveal capsules on most of the cells. However, all samples contained a small number (less than 1%) of cells surrounded by a halo of amorphous material that gradually thinned toward the periphery, giving the cells an ellipsoidal shape, as shown in Fig. 2A. The cells were located in the center of the ellipsoid and were difficult to see by TEM, because of the surrounding material. This general shape for the cell and the external material was verified by performing AFM measurements of the same cell (Fig. 2B). In agreement with the electron density measured in the TEM images, the thickness of the cells and external material gradually decreased from the center of the cell toward the periphery. When these cells were negatively stained with uranyl acetate (Fig. 2C), both the internal cell and the surrounding matrix shrunk when viewed using AFM (cf. Fig. 2B with D) to approximately one-half the height of the unstained whole mounts (Fig. 2E). Comparable shrinkage of the cell height upon staining was observed for cells with no visible surrounding halo. The shrinkage of the cell height upon staining was correlated with a significant reduction in the TEM image contrast (Fig. 2C). Nevertheless, the application of the stain resulted in improved TEM contrast for pili and flagella (data not shown). Additionally, multiple dendrite precipitates were observed as a result of the application of the stain. Since the halo of external material was observed using both TEM and AFM in unstained whole mounts and since a similar response of the halo to stain was observed using both techniques, its presence cannot be an artifact related to the application of the stain. We interpret the external halo material as capsular material surrounding the cell. Surprisingly, it was difficult to obtain TEM images after the staining procedure, because the Formvar film on the TEM grids tended to crack immediately after exposing cells to the electron beam. Since these regions had previously been scanned using AFM, the film cracking was most likely due to the mechanical stresses introduced by the AFM tip.

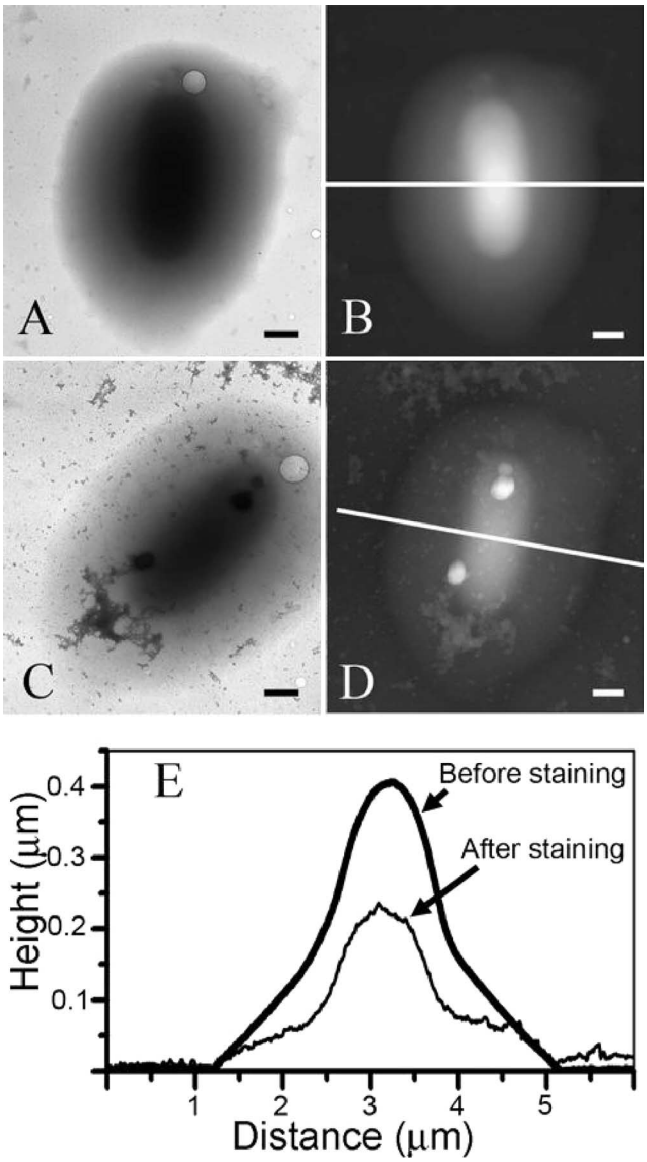

FIG. 2. (A and B) TEM image (A) and corresponding AFM topography image (B) of the same *S. oneidensis* MR-4 whole-cell mount on a free-standing Formvar film. (C and D) TEM and AFM images after the same cell was stained with uranyl acetate. (E) Topography profiles of the AFM images in panels B and D along the white lines. Bars, 500 nm.

AFM measurements of bacteria in liquid. There was poor adhesion by all four strains to glass slides coated with poly-L-lysine in HEPES buffer, and cells were easily displaced by the AFM tip in both contact and tapping modes during scanning, which made imaging difficult. In several cases, we were able to visualize the cells; however, there were multiple artifacts due to the line-by-line scanning caused by the limited degree of stiffness of the highly hydrated bacterial surface polysaccharides. Together, the poor cellular adhesion and low capsular

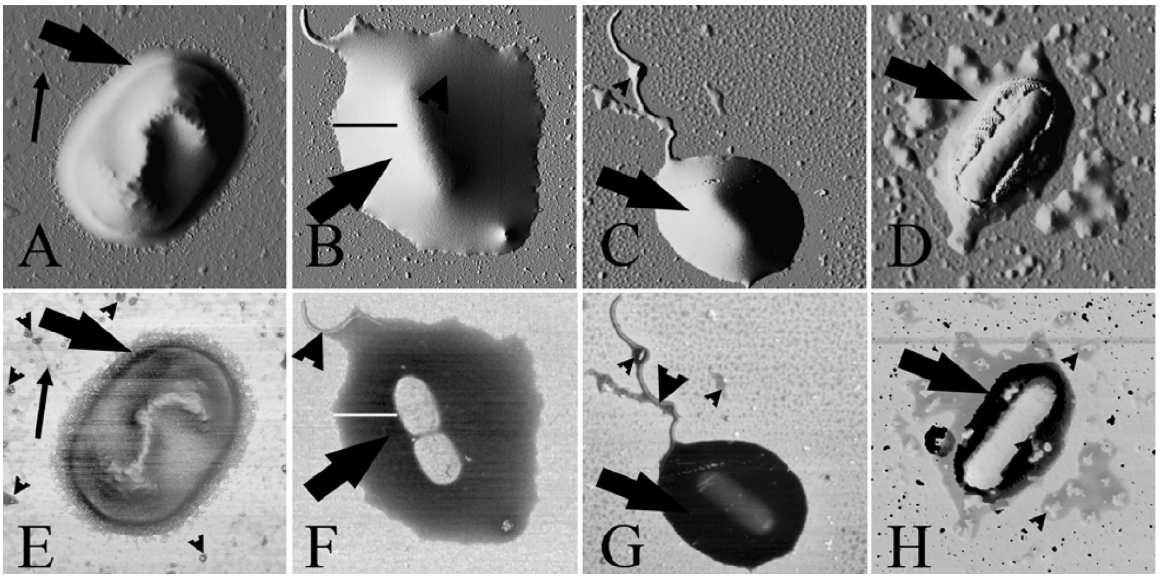

FIG. 3. AFM contrast-enhanced topography (A to D) and phase (E to H) images of encapsulated *E. coli* (A and E), *P. aeruginosa* (B and F), *S. oneidensis* MR-4 (C and G), and *G. sulfurreducens* PCA (D and H) bacterial cells dried onto mica. The AFM images were collected in low-frequency (21-kHz) tapping mode. The large arrows (all panels) indicate the capsular material, the small arrows in panels A and E indicate pili, the large arrowheads in panels F and G indicate flagella, and the small arrowheads in panels E, G, and H indicate pieces of capsular material that are separate from the bacterial cell, i.e., EPS. The black line in panel B and the white line in panel F were used to obtain the low-frequency tapping mode data shown in Fig. 4, below. The width of the images corresponds to a distance of 3.0 μm (A and E), 5.5 μm (B and F), 6.5 μm (C and G), and 5.0 μm (D and H).

stiffness limited the usefulness of AFM imaging of encapsulated bacteria in liquid (27). The measured FD curves indicated the presence of large repulsive forces (data not shown), which may indicate the presence of long polysaccharide molecules on the bacterial surface (1). No evidence for adhesion between the AFM tip and the bacterial capsule was observed on FD curves measured in HEPES buffer.

AFM measurements of bacteria in air. AFM on cells dried onto mica surfaces revealed that most of the bacteria that had adhered to the mica substrate were encapsulated in all four strains (*E. coli*, *P. aeruginosa*, *S. oneidensis*, and *G. sulfurreducens*). In many cases, the dried bacteria aggregated into clusters of cells. However, for the reliable determination of the properties of the capsules, we analyzed isolated cells, as shown in Fig. 3. Generally, it was difficult to identify the presence of a capsule on the basis of topography images alone. Instead, their presence was better revealed in phase images, in which the capsule appeared as a dark halo with phase angle values that were 15 to 35° smaller than those measured for the mica substrate (Fig. 3E, F, G, and H). The amount of the capsular material varied significantly between the cells within a given strain and, in the case of large capsules, the AFM images were very similar to those obtained for whole mounts of cells on TEM grids (Fig. 2B). The difference in the phase angle between the halo and the substrate allowed excellent visualization of the capsule surrounding each cell. The phase images also revealed each bacterium as a brighter object inside the capsular matrix, with phase angles that were approximately equal to those measured for the mica substrate. Only the outer capsular surface was observed in the corresponding topography images.

For all of the strains except *E. coli* K30, phase images revealed that the capsular matrix was a dense structure that was homogeneous on the length scales measured in this study. The outer surface of the capsular material was smooth and extended typically 300 to 500 nm beyond the periphery of each cell. The *E. coli* K30 capsule was thinner (150 to 200 nm) and possessed a rougher fibrous outer edge (Fig. 3A and E). We note that the phase contrast between the capsule and the *E. coli* K30 cell was much smaller than for the other bacterial strains.

Because the thickness of the capsule increased continuously from the outer edges of the capsule to the center of the cell (Fig. 2E), it was possible to correlate the local thickness of the capsule with the corresponding phase signal. This allowed us to probe the sensitivity of the phase angle values measured for the soft capsular material to the proximity of stiff objects underneath the surface of the capsule, e.g., the substrate and the bacterial cell. We also hypothesized that such depth sensitivity to the presence of stiff buried objects should depend on the resonance frequency and, correspondingly, on the stiffness of the cantilevers used for imaging. To determine the depth sensitivity, topography and phase images of *P. aeruginosa* FRD1 and *S. oneidensis* MR-4 bacteria were collected in both high- and low-frequency tapping modes. In Fig. 4A, we show the height values measured for a *P. aeruginosa* FRD1 cell along the black line in Fig. 3B, and in Fig. 4B we show the corresponding phase values measured for the same cell along the white line in Fig. 3F. In Fig. 4C, we plot the phase angles from Fig. 4B as a function of the corresponding capsule height from Fig. 4A to obtain the dependence of the measured phase angle on the thickness of the bacterial capsule. The depth sensitivity of the phase signal (i.e., the thickness at which the phase angle ceases to decrease with increasing thickness) was smaller for high-

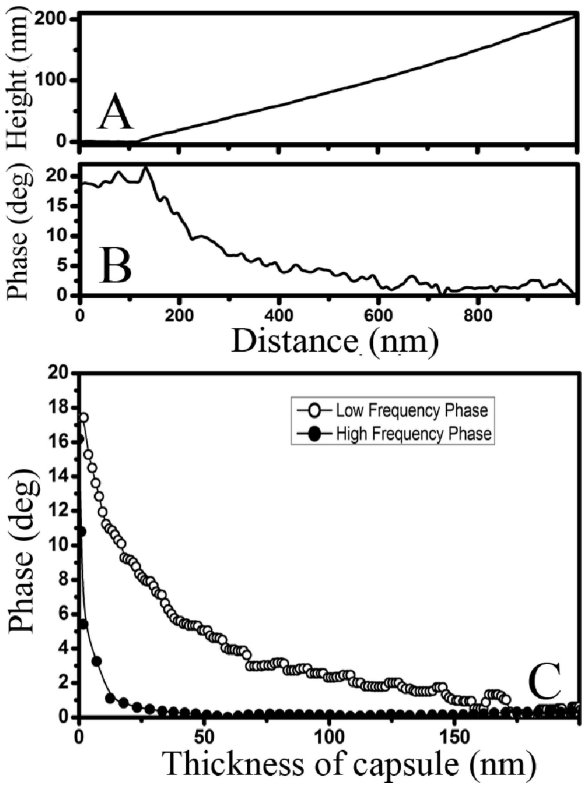

FIG. 4. (A and B) Profiles of the topography and phase images collected in low-frequency (21-kHz) tapping mode measured along the black line in Fig. 3B and the white line in Fig. 3F, respectively, for a *P. aeruginosa* FRD1 bacterial cell. (C) Dependence of the phase angle measured in AFM phase images on the thickness of the bacterial capsule of the same *P. aeruginosa* FRD1 bacterial cell, collected in both low-frequency (21-kHz) and high-frequency (300-kHz) tapping modes. Quantitatively similar results were obtained for *S. oneidensis* MR-4 bacteria.

frequency tapping (~50 nm) than for low-frequency tapping (~175 nm).

Curves similar to Fig. 4 can be used as a calibration for the depth sensitivity of the phase signal and, using this calibration, the thickness of the capsular matrix on top of the bacteria can be estimated. Assuming that bacteria are relatively hard particles (since only a small, 1 to 2° difference in the phase angle was observed between the mica substrate and nonencapsulated bacteria), the thickness of the matrix can be estimated to be 10 to 12 nm at the center of the bacterial cell shown in Fig. 3G. For the cell shown in Fig. 3H, the thickness values could not be determined reliably due to the small difference between the phase angles measured on the mica and bacterium.

Phase images also revealed the presence of flagella and pili in all strains studied. In addition, particles with diameters of >100 nm, which appeared as dark objects in the phase images, were frequently seen surrounding the cells beyond the capsule, suggesting that they had budded from the capsule and, since they were now completely separated from the cell, they could be considered to be EPS. It is more difficult to assess the contrast associated with particles smaller than 10 nm because of the spatial resolution used in the AFM measurements in the present study. In most cases, small particles with diameters of 10 to 80 nm, which are presumably membrane vesicles and/or protein aggregates, were clearly visible as bright spots of larger phase angle. These were often contained within the darker EPS patches. Significantly larger amounts of EPS were observed for *P. aeruginosa* FRD1 and *G. sulfurreducens* PCA cells compared to the other strains.

Two control experiments were also performed to further investigate the phase contrast between the bacterial capsules and the mica substrate. In control experiment I, the effect of the HEPES buffer on the phase contrast was measured by comparing cells rinsed with MilliQ water to those which had only been exposed to HEPES buffer. We observed that the phase contrast was significantly smaller (3 to 4°) for the cells rinsed in MilliQ water than for those which had only been exposed to HEPES buffer (15 to 35°). In control experiment II, we measured the phase contrast between the bacterial capsules and the mica substrate as a function of exposure time to ambient environmental conditions. We found that the phase contrast decreased from ~30° to ~10° after several hours of continuous exposure to ambient environmental conditions.

DISCUSSION

Observations by TEM. TEM is invaluable for high-resolution imaging of bacteria and their components. However, the present study demonstrates that some TEM techniques are not necessarily well-suited for the study of bacterial capsules. In particular, in TEM analysis of whole-cell mount preparations, the halo that we attributed to the capsular matrix was visible on only a small number of cells on each TEM grid. In contrast, TEM of freeze-substitution preparations and AFM measurements performed on cells on mica substrates showed that most cells possessed well-defined capsules. This result suggests that encapsulated cells with hydrophilic capsules do not tend to adhere to the hydrophobic Formvar film suspended over the TEM grid, and therefore this sample preparation technique is not effective for the study of encapsulated cells. We have also shown that although the relatively common Ruthenium red embedding technique (6) revealed a capsule in *E. coli* K30 and *P. aeruginosa* FRD1, it did not do so for *S. oneidensis* MR-4 and *G. sulfurreducens* PCA. The more sophisticated freeze-substitution preparations for TEM did not reveal a capsule on *G. sulfurreducens* PCA. In contrast, AFM phase imaging revealed that all of the bacterial strains have some encapsulated cells.

It is possible that one of the problems attributable to detecting capsules with TEM is due to the overall charge character of the polymers that make up the matrix. For example, Ruthenium red embeddings of *S. oneidensis* MR-4 did not reveal a capsule. This may be attributed to the lower electronegativity under physiological conditions of its CPS, since only one of five repeating units of its CPS molecules possesses a negative charge (41). In contrast, both *E. coli* K30 and *P. aeruginosa* FRD1 produce highly acidic polysaccharides (30) that readily bind heavy metal stains. Another indication from TEM of thin sections that capsules are present but not readily observable in *S. oneidensis* is that, although cells situate themselves close to one another, they never actually contact each other (Fig. 1C); the condensed capsule must be holding them apart even if it is unstained. Typically, both conventional and freeze-substituted

preparations produce samples in which the nonencapsulated cells contact each other via their outer membranes (Fig. 1E). This occurs because cells are commonly collected by centrifugation and are therefore densely packed. Encapsulated bacteria will contact each other via the outer part of their capsule. Because the cells are not in direct contact in conventional embeddings of *E. coli* K30 (Fig. 1A) and *P. aeruginosa* FRD1 (Fig. 1B), there may be shrinkage of the capsule matrix during sample preparation. In embeddings, shrinkage probably occurs during both the staining and dehydration processes. During staining, multivalent heavy metal stains (e.g., Ruthenium red and uranyl acetate) must attach to the charged CPS polymers so as to salt-bridge and condense them. Dehydration, on the other hand, displaces water from the capsular matrix, which accounts for often over 95% of the mass of the capsule, thereby shrinking it. There was capsule shrinkage even in negative stains of whole cells (Fig. 2E), which confirmed that seen with embeddings described above. In contrast, capsules were preserved in freeze-substitutions of *E. coli* K30, *P. aeruginosa* FRD1, and *S. oneidensis* MR-4 (Fig. 1E). Freeze-substitution is a cryo-technique that relies on the almost instantaneous physical preservation of structure during vitrification (6); there may be some subsequent alteration in capsule preservation when samples are chemically substituted and embedded in plastic for thin sectioning, but these preparations must be a reasonably accurate representation of capsules close to their natural hydrated state.

In most freeze-substitutions, the CPS appeared to be homogeneously stained across the thickness of the capsule, with a rough outer edge. An inhomogeneous fibrous structure had been observed previously for CPS molecules during freeze-substitution (18), but we observed such a fibrous structure in only a few samples. It is possible that the fibrous structure is an artifact resulting from the collapse or aggregation of polysaccharide molecules into fibers, or it indicates subtle chemical differences between capsule chemotypes that are genus or strain specific. Better preservation of capsules was probably achieved in the present study due to our improved control over vitrification by using an automated high-pressure freezer and control over freeze-substitution by using a temperature-stepped freeze-substitution apparatus (see Materials and Methods).

Our combined AFM and TEM data on whole-mount preparations also indicate that staining is an unnecessary procedure for the detection of capsules. We found that a negative stain can actually degrade TEM image quality by shrinking the capsule by up to 40% of its height, based on the AFM measurements.

Observations by AFM. The phase contrast observed in AFM is normally attributed to the dissipation of the energy of the vibrating cantilever due to adhesive interactions during intermittent contact between the AFM tip and the sample surface (10, 16), as well as the local viscoelastic properties of the sample. Typically, the energy dissipation is due to both of these factors, and separating these contributions is difficult for soft polymeric materials. For AFM measurements performed in air, the situation is further complicated by the presence of capillary forces on the AFM tip due to the presence of a thin water layer at almost any solid-air interface. This is especially true in the case of hydrophilic materials, such as soft biological materials. As a result, the quantitative interpretation of AFM phase images is complicated, and phase images are typically discussed by comparing the phase angle measured at different positions on the sample surface. The usefulness of phase imaging for visualizing regions of different stiffness on a sample is well-established for microstructural studies of phase-separated polymeric materials and polymer composites (10). In these studies, domains of different polymers or nanoparticles and microparticles embedded within polymers can be unambiguously identified in AFM phase images due to differences in the local material stiffness.

In the present study, the AFM tip interacts with the bacterial capsule, which is typically a highly hydrated, deformable gel. In tapping mode, the tip is in contact with the sample surface during only a small portion of the vibration cycle. It is likely that contact is made with the surface water layer, and a small penetration of the tip into the capsular material is obtained during each oscillation of the cantilever. The phase contrast of the capsule is caused by the simultaneous action of large capillary forces and viscous damping of the cantilever vibration during its contact with the capsule surface. This complex interaction between the AFM tip and the capsule also gives rise to complicated shapes for the FD curves collected on such capsules (O. Stukalov, A. Korenevsky, T. J. Beveridge, and J. R. Dutcher, unpublished data).

During the process of extended desiccation, the capsules dehydrate and solidify and, as a result, the phase contrast between the mica and the capsules decreases, as observed in control experiment II. This result indicates that the phase contrast can be used as a measure of the hydration state of the capsule and may be potentially useful in studies of resistance of bacteria to desiccation.

AFM cantilevers that are used for the low-frequency tapping mode are softer than those used for the high-frequency tapping mode, such that the contact time between the AFM tip and the sample surface is longer. This results in increased penetration of the tip into the capsular matrix. As a result, low-frequency tapping is more sensitive to contrast at larger depths than high-frequency tapping (Fig. 4): ~175-nm depth sensitivity for low-frequency (21 kHz) tapping measurements versus a ~50-nm depth sensitivity for high-frequency (300 kHz) tapping measurements. A similar value of 80 nm for the depth sensitivity of AFM phase imaging was obtained by Bodiguel et al. (7) for silica nanoparticles buried in a polyethylacrylate elastomer and using cantilevers with a resonance frequency of ~160 kHz.

We found that the phase contrast between the bacterial capsule and the surrounding mica substrate was much smaller for bacteria rinsed in MilliQ water than for bacteria which had only been exposed to HEPES buffer. This result indicates that the presence of HEPES buffer, even in very small concentrations (2 mM in our case), significantly affects the mechanical properties of the capsules. The higher phase contrast observed for bacterial capsules exposed to HEPES buffer is consistent with AFM phase imaging of *Salmonella enterica* serovar Typhimurium, for which it was observed that rinsing the bacteria with HEPES buffer could stabilize and promote capsule formation (35). It is likely that molecules from the HEPES buffer are trapped in the capsular matrix and may not be completely removed during rinsing with MilliQ water. It is quite possible that HEPES molecules interact with proteins that may be

trapped in the capsular matrix, e.g., products of cell metabolism, since HEPES buffer is often found to be a binding and stabilizing agent in protein crystals (13). Therefore, HEPES buffer could significantly modify the properties of the capsular matrix.

In conclusion, we have found that TEM does not always give an accurate appraisal of encapsulated bacteria and can be unreliable, especially if a cryo-technique such as freeze substitution is not used. AFM imaging of bacteria dried onto mica is an excellent technique for the detection and characterization of bacterial capsules. AFM offers the ability to measure the phase of the cantilever vibrations, the nanoscale topography of the bacterial cells, and the interaction between the AFM tip and the surface through measurement of AFM phase images and FD curves. In contrast to standard TEM imaging techniques, AFM phase imaging performed in air on bacterial cells revealed the presence of capsules for all bacterial strains used in the present study and also revealed that bacterial capsules remain in a highly deformable state for several hours under ambient conditions. In addition, AFM phase imaging visualized the bacteria underneath the capsular material, with a depth sensitivity that decreased with increasing tapping frequency. The striking softening effect of a very small amount of HEPES buffer on the properties of the capsules, accompanied by an enhanced phase contrast in AFM, could potentially be exploited in studies of interactions of the capsular matrix with cations and other small molecules. Yet, it is difficult to completely discount the utility of TEM since it is still the only current method that can visualize the minute cytoplasmic components within cells and distinguish the sequential layering of cell envelope structures in relation to external matrices such as capsules and EPS. The very best studies should utilize a combination of approaches that are determined by the information required but, certainly, a combination of AFM and TEM is a combination that excels for bacterial capsules.

ACKNOWLEDGMENTS

We gratefully acknowledge financial support from the Advanced Foods and Materials Network (AFMnet), the Canadian Foundation for Innovation, and NSERC to J.R.D. and T.J.B. and from the U.S. Department of Energy and the Grand Challenge in Biogeochemistry Program to T.J.B. The TEM experiments were performed in the NSERC Guelph Regional Integrated Imaging Facility, which is partially funded by an NSERC Major Facility Access grant to T.J.B. J.R.D. and T.J.B. acknowledge support from the Canada Research Chairs program.

REFERENCES

1. **Abu-Lail, N. I., and T. A. Camesano.** 2003. Role of ionic strength on the relationship of biopolymer conformation, DLVO contributions, and steric interactions to bioadhesion of *Pseudomonas putida* KT2442. Biomacromolecules **4:**1000–1012.
2. **Arnoldi, M., M. Fritz, E. Bäuerlein, M. Radmacher, E. Sackmann, and A. Boulbitch.** 2000. Bacterial turgor pressure can be measured by atomic force microscopy. Physiol. Rev. **62:**1034–1044.
3. **Bayer, M. E.** 1990. Visualization of the bacterial polysaccharide capsule, p. 129–157. *In* K. Jann and B. Jann (ed.), Bacterial capsules. Springer-Verlag, Berlin, Germany.
4. **Bayer, M. E., and H. Thurow.** 1977. Polysaccharide capsule of *Escherichia coli*: microscope study of its size, structure, and sites of synthesis. J. Bacteriol. **130:**911–936.
5. **Beveridge, T. J., D. Moyles, and B. Harris.** 2007. Electron microscopy, p. 54–81. *In* C. A. Reddy, T. J. Beveridge, J. A. Breznak, G. A. Marzluf, T. M. Schmidt, and L. R. Snyder (ed.), Methods for general and molecular microbiology, 3rd ed. ASM Press, Washington, DC.
6. **Beveridge, T. J., J. R. Lawrence, and R. G. E. Murray.** 2007. Sampling and staining for light microscopy, p. 19–33. *In* C. A. Reddy, T. J. Beveridge, J. A. Breznak, G. A. Marzluf, T. M. Schmidt, and L. R. Snyder (ed.), Methods for general and molecular microbiology, 3rd ed. ASM Press, Washington, DC.
7. **Bodiguel, H., H. Montes, and C. Freitigny.** 2004. Depth sensing and dissipation in tapping mode atomic force microscopy. Rev. Sci. Instrum. **75:**2529–2535.
8. **Bolshakova, A. V., O. I. Kiselyova, A. S. Filononv, O. Yu. Frolova, Y. L. Lyubchenko, and I. V. Yaminsky.** 2001. Comparative studies of bacteria with an atomic force microscopy operating in different modes. Ultramicroscopy **86:**121–128.
9. **Butt, H.-J., B. Cappella, and M. Kappl.** 2005. Force measurements with the atomic force microscope: technique, interpretation and applications. Surf. Sci. Rep. **59:**1–152.
10. **Chernoff, D. A., and S. Magonov.** 2003. Atomic force microscopy, p. 490–531. *In* R. F. Bradly, Jr. (ed.), The comprehensive desk reference of polymer characterization and analysis. American Chemical Society/Oxford University Press, Oxford, United Kingdom.
11. **Coppi, M. V., C. Leang, S. J. Sandler, and D. R. Lovley.** 2001. Development of a genetic system for *Geobacter sulfurreducens*. Appl. Environ. Microbiol. **67:**3180–3187.
12. **Cowman, M. K., C. Spagnoli, D. Kudasheva, M. Li, A. Dyal, S. Kanai, and E. A. Balazs.** 2005. Extended, relaxed, and condensed conformations of hyaluronan observed by atomic force microscopy. Biophys. J. **88:**590–602.
13. **Crennell, S. J., G. O. Hreggvidsson, and E. Nordberg Karlsson.** 2002. The structure of *Rhodothermus marinus* Cel12a, a highly thermostable family 12 endoglucanase, at 1.8 Å resolution. J. Mol. Biol. **320:**883–897.
14. **Dufrêne, Y. F.** 2004. Using nanotechniques to explore microbial surfaces. Nat. Rev. Microbiol. **2:**451–460.
15. **Fang, H. H. P., K. Y. Chan, and L.-C. Xu.** 2000. Quantification of bacterial adhesion forces using AFM. J. Microbiol. Methods **40:**89–97.
16. **Garcia, R., R. Magerle, and R. Perez.** 2007. Nanoscale compositional mapping with gentle forces. Nat. Mater. **6:**405–411.
17. **Geesey, G. G., and L. Jang.** 1989. Interactions between metal ions and capsular polymers, p. 325–357. *In* T. J. Beveridge and R. J. Doyle (ed.), Metal ions and bacteria. Wiley, New York, NY.
18. **Graham, L. L., R. Harris, W. Villiger, and T. J. Beveridge.** 1991. Freeze-substitution of gram-negative eubacteria: general cell morphology and envelope profiles. J. Bacteriol. **173:**1623–1633.
19. **Hanna, A., M. Berg, V. Stout, and A. Razatos.** 2003. Role of capsular colonic acid in adhesion of uropathogenic *Escherichia coli*. Appl. Environ. Microbiol. **69:**4474–4481.
20. **Hunter, R. C., and T. J. Beveridge.** 2005. High-resolution visualization of *Pseudomonas aeruginosa* PAO1 biofilms by freeze-substitution transmission electron microscopy. J. Bacteriol. **187:**7619–7630.
21. **Karlyshev, A. V., M. V. McCrossan, and B. W. Wren.** 2001. Demonstration of polysaccharide capsule in *Campylobacter jejuni* using electron microscopy. Infect. Immun. **69:**5921–5924.
22. **Korenevsky, A. A., E. Vinogradov, Y. Gorby, and T. J. Beveridge.** 2002. Characterization of the lipopolysaccharides and capsules of *Shewanella* spp. Appl. Environ. Microbiol. **68:**4653–4657.
23. **Korenevsky, A., and T. J. Beveridge.** 2007. The surface physicochemistry and adhesiveness of *Shewanella* are affected by their surface polysaccharides. Microbiology **153:**1872–1883.
24. **Lovley, D. R., D. E. Holmes, and K. P. Nevin.** 2004. Dissimilatory Fe(III) and Mn(IV) reduction. Adv. Microb. Physiol. **49:**219–286.
25. **May, T. B., D. Shinabarger, R. Maharaj, J. Kato, L. Chu, J. D. DeVault, S. Roychoudhury, N. A. Zielinski, A. Berry, and R. K. Rothmel.** 1991. Alginate synthesis by *Pseudomonas aeruginosa*: a key pathogenic factor in chronic pulmonary infections of cystic fibrosis patients. Clin. Microbiol. Rev. **4:**191–206.
26. **Nozue, H., T. Hayashi, Y. Hashimoto, T. Ezaki, K. Hamasaki, K. Ohwada, and Y. Terawaki.** 1992. Isolation and characterization of *Shewanella alga* from human clinical specimens and emendation of the description of *S. alga* Simidu *et al.*, 1990, 335. Int. J. Syst. Bacteriol. **42:**628–634.
27. **Obst, M., and M. Dittrich.** 2005. Living under an atomic force microscope. An optimized approach for in vivo investigations on surface alterations towards biomineral nucleation on cyanobacterial cells. Geobiology **3:**179–193.
28. **Ophir, T., and D. Gutnick.** 1994. A role of exopolysaccharides in the protection of microorganisms from desiccation. Appl. Environ. Microbiol. **60:**740–745.
29. **Pembrey, R. S., K. C. Marshall, and R. P. Schneider.** 1999. Cell surface analysis techniques: what do cell preparation protocols do to cell surface properties? Appl. Environ. Microbiol. **65:**2877–2894.
30. **Roberts, I. R.** 1996. The biochemistry and genetics of capsular polysaccharide production in bacteria. Annu. Rev. Microbiol. **50:**285–315.
31. **Sara, M., D. Pum, B. Schuster, and U. B. Sleytr.** 2005. S-layers as patterning elements for application in nanobiotechnology. J. Nanosci. Nanotechnol. **5:**1939–1953.
32. **Schaer-Zammaretti, P., and J. Ubbink.** 2003. Imaging of lactic acid bacteria with AFM—elasticity and adhesion maps and their relationship to biological and structural data. Ultramicroscopy **97:**199–208.

33. **Schembri, M. A., D. Dalsgaard, and P. Klemm.** 2004. Capsule shields the function of short bacterial adhesions. J. Bacteriol. **186:**1249–1257.
34. **Sletmoen, M., G. Maurstad, P. Sikorski, B. S. Paulsen, and B. T. Stokke.** 2003. Characterisation of bacterial polysaccharides: steps towards single-molecular studies. Carbohydr. Res. **338:**2459–2475.
35. **Suo, Z., X. Yang, R. Avci, L. Kellerman, D. W. Pascual, M. Freis, and A. Steele.** 2007. HEPES-stabilized encapsulation of *Salmonella typhimurium*. Langmuir **23:**1365–1374.
36. **Touhami, A., M. H. Jericho, and T. J. Beveridge.** 2004. Atomic force microscopy of cell growth and division in *Staphylococcus aureus*. J. Bacteriol. **186:**3286–3295.
37. **Touhami, A., M. H. Jericho, J. M. Boyd, and T. J. Beveridge.** 2006. Nanoscale characterization and determination of adhesion forces of *Pseudomonas aeruginosa* pili by using atomic force microscopy. J. Bacteriol. **188:**370–377.
38. **Ubbink, J., and P. Schär-Zammaretti.** 2005. Probing bacterial interactions: integrated approaches combining atomic force microscopy, electron microscopy and biophysical techniques. Micron **36:**293–320.
39. **Vadillo-Rodriguez, V., H. J. Busscher, W. Norde, J. de Vries, and H. C. van der Mei.** 2004. Relations between macroscopic and microscopic adhesion of *Streptococcus mitis* strains to surfaces. Microbiology **150:**1015–1022.
40. **Vinogradov, E., A. Korenevsky, D. Lovley, and T. J. Beveridge.** 2004. The structure of the core region of the lipopolysaccharide from *Geobacter sulfurreducens*. Carbohydr. Res. **339:**2901–2904.
41. **Vinogradov, E., L. Nossova, A. Korenevsky, and T. J. Beveridge.** 2005. The structure of the capsular polysaccharide of *Shewanella oneidensis* strain MR-4. Carbohydr. Res. **340:**1750–1753.
42. **Vogel, B. F., K. Venkateswaran, M. Satomi, and L. Gram.** 2005. Identification of *Shewanella baltica* as the most important H_2S-producing species during iced storage of Danish marine fish. Appl. Environ. Microbiol. **71:**6689–6697.
43. **Whitfield, C., and I. S. Roberts.** 1999. Structure, assembly and regulation of expression of capsules in *Escherichia coli*. Mol. Microbiol. **31:**1307–1319.
44. **Yao, X., J. Walter, S. Burke, S. Stewart, M. H. Jericho, D. Pink, R. Hunter, and T. J. Beveridge.** 2002. Atomic force microscopy and theoretical considerations of surface properties and turgor pressures of bacteria. Colloids Surf. B **23:**213–230.
45. **Yao, X., M. H. Jericho, D. Pink, and T. J. Beveridge.** 1999. Thickness and elasticity of gram-negative murein sacculi measured by atomic force microscopy. J. Bacteriol. **181:**6865–6875.